Journal of Alloys and Compounds 509 (2011) 7198–7204

Contents lists available at ScienceDirect

Journal of Alloys and Compounds

journal homepage: www.elsevier.com/locate/jallcom

Electronic structure and optical property of $As_2(Te_{1-x}S_x)_3$ and $As_2(Te_{1-x}Se_x)_3$ crystals

Ching-Hwa Ho [a,b,*]

[a] Graduate Institute of Engineering, Graduate Institute of Applied Technology, National Taiwan University of Science and Technology, Taipei 106, Taiwan
[b] Department of Electronic Engineering, National Taiwan University of Science and Technology, Taipei 106, Taiwan

ARTICLE INFO

Article history:
Received 21 January 2011
Received in revised form 5 April 2011
Accepted 14 April 2011
Available online 20 April 2011

Keywords:
Arsenic chalcogenides
Thermoreflectance

ABSTRACT

Single crystals of S- and Se-incorporated As_2Te_3 have been grown by vertical Bridgman method. The electronic structure and optical property of $As_2(Te_{1-x}S_x)_3$ [ATS] and $As_2(Te_{1-x}Se_x)_3$ [ATSe] series compounds have been characterized experimentally by thermoreflectance (TR) measurements in a wide energy range of 0.7–6 eV. X-ray diffraction measurements showed that the diffraction peaks of sulfur- and selenium-incorporated $As_2(Te_{1-x}S_x)_3$ $0 \le x \le 0.3$ and $As_2(Te_{1-x}Se_x)_3$ $0 \le x \le 0.6$ crystals shift to higher diffraction angles with the increase of the sulfur or selenium incorporations. The analysis of X-ray measurement revealed similar crystalline phase for the As_2Te_3 and those of the S- or Se-incorporated As_2Te_3. The experimental TR spectra of $As_2(Te_{1-x}S_x)_3$ $(0 \le x \le 1)$ and $As_2(Te_{1-x}Se_x)_3$ $(0 \le x \le 1)$ exhibit a lot of derivative-like spectral features in the vicinity of band edge as well as in the higher-lying bands. Transition energies and broadening parameters of the TR features at 40 and 300 K were analyzed. Compositional dependences of band gap and interband transition energies of the ATS and ATSe series were evaluated. The origins for the interband transitions in the ATS and ATSe are assigned. Based on the experimental analyses, the electronic structure of the diarsenic trichalcogenides, $As_2(Te_{1-x}Se_x)_3$ and $As_2(Te_{1-x}S_x)_3$, is hence being realized.

1. Introduction

Arsenic chalcogenides have recently received considerable interests in optics and materials researches because their intriguing properties in electronic structure and crystallographic ordering. As_2Te_3 (amorphous or crystalline state) belongs to one of the multicomponent chalcogenides system that exhibited a specific character of electrical threshold and memorial switching [1]. It was suggested to be a promising candidate for fabrication of optical memory devices [2]. The optical gap for the diarsenic tritelluride As_2Te_3 was announced to be in the range of 0.95–0.98 eV with energy variation in between the parabolic band states [3]. One of the stable crystalline phases for As_2Te_3 is α-As_2Te_3, which is a monoclinic structure with $C_{2h}{}^3$–$C2/m$ symmetry [4]. The other stabilized phase for the crystalline As_2Te_3 is a rhombohedral Bi_2Te_3-type structure with $\bar{R}3m$ symmetry (i.e. β-As_2Te_3) [5]. The crystal structure of α-As_2Te_3 shows a little bit difference in atomic arrangement as comparing to that of the "orpiment" structure in As_2Se_3 and As_2S_3 [6,7].

As_2Se_3 and As_2S_3 are diamagnetic semiconductors that crystallized in layer-type structure of monoclinic symmetry (space group: $C_{2h}{}^5$-$P2_1/n$) [7,8]. The "orpiment", As_2S_3, is a common mineral on earth. For the growth of As_2S_3 single crystal, the synthesized compound shows much difficulty to crystallize from the As-S melt because the cooling of As_2S_3 melts usually results in formation a lot of glassy solids. However, the glassy diarsenic trichalcogenides showed a special character of photo-induced structural change when a light beam impinges on these glasses [9,10]. The character of optical-induced structural transformation makes these glassy chalcogenides own a potential usage for being a photosensitive material applied in optical data recording [11]. Crystalline As_2S_3 and As_2Se_3 belong to a direct semiconductor. The energy gaps were reported to be 2.6 eV for As_2S_3 [7] and 1.75 eV for As_2Se_3 [12] at 300 K. The reported gap value for As_2Te_3 is around 0.9 eV [7]. However, very rare evidence can be found to verify the gap values of As_2X_3 (X = S, Se, and Te). From the band-edge property of the As_2X_3, it is inferred that the crystalline $As_2(Te_{1-x}S_x)_3$ [ATS] $(0 \le x \le 1)$ and $As_2(Te_{1-x}Se_x)_3$ [ATSe] $(0 \le x \le 1)$ systems are maybe a direct semiconductor, in which the energies of band gaps in the ATS and ATSe systems can render them possess the potential ability for fabrication of optoelectronics devices applied in near infrared (NIR) to visible region. To get better understanding on the optical characteristic of the arsenic chalcogenides, the band-edge structure and

* Correspondence address: Graduate Institute of Engineering, Graduate Institute of Applied Technology, 43 Sec. 4, Keelung Rd., Taipei 106, Taiwan.
E-mail address: chho@mail.ntust.edu.tw

0925-8388/$ – see front matter © 2011 Elsevier B.V. All rights reserved.
doi:10.1016/j.jallcom.2011.04.061

electronic structure in whole series of ATS and ATSe crystalline systems could be crucial and which need to be explored.

In this paper, we probe the electronic structure of whole series ATS and ATSe chalcogenide systems using thermoreflectance measurements in a wide energy range from NIR to ultraviolet (UV) region. The experiments were carried out at 40 and 300 K. The TR spectra for the chalcogenides were analyzed by a Lorentzian line-shape function. The experimental analyses confirmed that the whole series ATS and ATSe are direct semiconductors. The experimental TR results also indicated that the band-edge nature for the valence and conduction bands of the ATSe and ATS is similar. Compositional dependences of transition energies of the ATSe and ATS systems are evaluated. The dependences of the electronic structures of the diarsenic trichalcogenides are analyzed and discussed.

2. Experimental

Single crystals of Se- and S-incorporated As_2Te_3 with different stoichiometric compositions were grown by vertical Bridgman (VB) method [13]. The source materials for the crystalline chalcogenides were prepared by synthesizing $As_2(Te_{1-x}Se_x)_3$ and $As_2(Te_{1-x}S_x)_3$ with different alloy compositions. Appropriate amounts of arsenic, tellurium, selenium and sulfur with 99.999% purity were put into a carbon-coated ampoule of 1.0 cm inner diameter (ID), which was then evacuated and sealed under vacuum. The quartz ampoule was slowly heated to the melting point of ~850 °C for the synthesized material in a rocking furnace and held at the melting temperature for two days. At the end of the process the ampoule was quenched to room temperature. For VB growth, the ampoule was pre-heated to the melting point. The descending rate of the quartz ampoule in the vertical furnace was about 1.0 mm per hour and the temperature gradient was set greater than −45 °C/cm from hot zone to cold area in the furnace. In order to achieve temperature uniformity the quartz ampoule was rotated at a constant speed of 15 cycles/min in the vertical furnace. Growing high S-contained crystal was considerably more difficult than the other chalcogenides due to high sulfur pressure induced in the quartz ampoule with liquid-phase growth. Even a very low growth rate, a lot of glassy chalcogenides were formed in the $As_2(Te_{1-x}S_x)_3$ series compounds with $x > 0.3$. However, after several rounds of growing process, the crystalline ATSe and ATS solids with $x = 0$, 0.4, 0.6, and 1 for $As_2(Te_{1-x}Se_x)_3$ and $x = 0$, 0.1, and 0.3 for $As_2(Te_{1-x}S_x)_3$ were also obtained. The as-grown crystals of arsenic chalcogenides are essentially layer type with a thicknesses of 30–90 μm and a surface area of about 15 mm^2. There is also a smaller layer crystal of As_2S_3 with surface area of ~0.25 mm^2 obtained from the VB growth. It is available for TR measurement.

For X-ray studies, several small crystals from each batch of $As_2(Te_{1-x}Se_x)_3$ ($x = 0$, 0.4, and 0.6) and $As_2(Te_{1-x}S_x)_3$ ($x = 0$, 0.1, and 0.3) were finely ground and the X-ray powder patterns were taken and recorded by means of a slow moving radiation detector. The copper Kα radiation (λ = 1.542 Å) was employed in the X-ray diffraction measurements and a silicon standard was used for the experimental calibration. The lattice constants for the ATSe and ATS series solids with reasonable standard error were obtained by the least-square fits of a Jandel SigmaPlot mathematical software [14].

The TR experiments were done in a wide energy range from 0.7 to 6 eV. An 150 W halogen lamp filtered by a PTI 0.2 m monochromator provided the monochromatic light for the NIR portion while an 150 W xenon-arc lamp was the light source in the visible to UV region. A Thorlab PDA400 InGaAs detector (0.7–1.3 eV portion) and an EG&G HUV 2000B silicon photodiode (1.3–2 eV) were used for the lower energy detection. A Hamamatsu photomultiplier tube acted as the optical detector in the higher-energy range (2–6 eV). Phase-sensitive detection was employed for the TR measurement and the AC signal was recorded from an EG&G model 7265 dual phase lock-in amplifier. For thermal perturbation of the samples, a quartz substrate acted as the heat sink [15]. The glass substrate was coated with a winding strip of golden tracks acting as the heating element. The shape of the golden strip was formed by a copper mask. The heating path consists of two wide tracks at the end sections and one narrow track lying in between them. The narrow track in the middle section is designed to act as a heat generation source when electrical current passes through the heater. The wide tracks at the end sections facilitate the heat dissipation when electrical power is off. The layered samples were closely attached on the narrow track of the Au path by silicone grease. Thermal modulation of the sample was achieved by indirect heating with supplying the current pulses to the Au heating path periodically. Heating pulses of low frequency and long duty cycle seem to be more efficient in enhancing the spectral amplitude of the transition feature. The heat generation and dissipation from the Au tracks on quartz substrate must be well balanced to avoid any increase of temperatures on sample (i.e. weak heating disturbance). Low temperature TR measurements were carried out at 40 K. A RMC model 22 closed-cycle cryogenic refrigerator equipped a digital thermometer controller facilitated the low-temperature measurements.

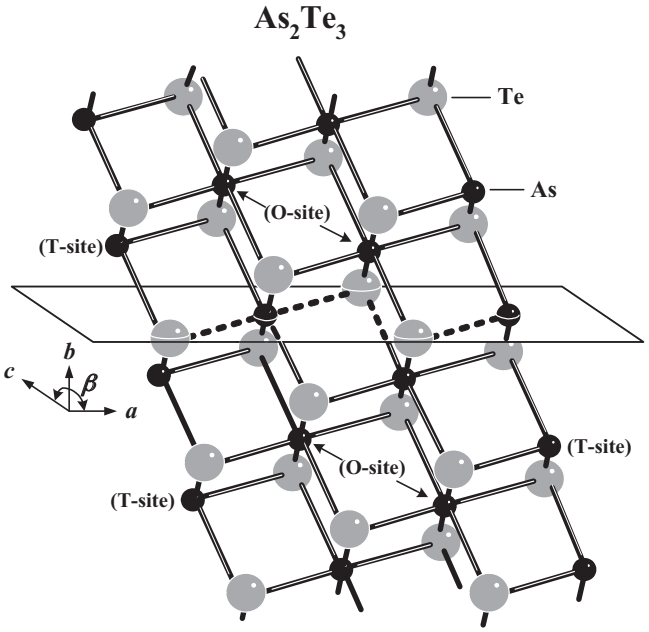

Fig. 1. The schematic representation of crystal structure of monoclinic As_2Te_3 ($C2/m$). All the Te atoms are threefold coordinated and the As atoms are either tetrahedrally (T-sites) or octahedrally (O-sites) coordinated (Ref. [4]).

3. Results and discussion

The schematic representation of monoclinic structure for As_2Te_3 is depicted in Fig. 1 [4,16]. The structure consists of two non-equivalent arsenic positions and three non-equivalent tellurium positions in its crystallographic arrangement. Two adjacent octahedra share the tellurium edges and align in ~[1 0 3] direction of the monoclinic As_2Te_3. All the tellurium atoms are nearly threefold coordinated and arsenic atoms are either tetrahedrally (T-sites) or octahedrally (O-sites) coordinated in the monoclinic As_2Te_3. The T-site As atoms are strongly bound to three neighboring Te atoms in a trigonal pyramidal configuration, whereas the O-site As atoms are octahedrally coordinated by Te atoms. The polyhedra form double chains capped by T-site As atoms, and the complex chains are parallel to the binary axis of the monoclinic cell, which inter-attracts by weak van der Waals force along the [1 0 0] direction. It also means a good cleavage property existed in between the individual layer plane of As_2Te_3.

Fig. 2(a) and (b) shows the X-ray diffraction patterns of S- and Se-incorporated As_2Te_3 compounds: $As_2(Te_{1-x}S_x)_3$ with $x = 0$, 0.1, and 0.3, and $As_2(Te_{1-x}Se_x)_3$ with $x = 0$, 0.4, and 0.6, respectively. A lot of diffraction peaks are found in the angular range of $2\Theta = 20$–$60°$ due to lower-symmetry nature of the monoclinic arsenic chalcogenides. The diffraction peaks of As_2Te_3 are quite similar to the previously reported data by Carron [16]. The as-grown As_2Te_3 crystals are single phase and crystallized in the monoclinic structure of $C_{2h}{}^3$–C2/m symmetry (α-As_2Te_3) [16]. For the X-ray diffraction data of $As_2(Te_{0.9}S_{0.1})_3$ and $As_2(Te_{0.7}S_{0.3})_3$ shown in Fig. 2(a), many characteristic peaks are the same as those detected for the As_2Te_3 crystal. The peak features of the diffraction curves for the S-incorporated ATS samples show slight shift to higher diffraction angle with the increase of the sulfur incorporation. A small change in lattice constant occurs in sulfur incorporated $As_2(Te_{1-x}S_x)_3$ with $x = 0.1$ and $x = 0.3$. It is also shown in Fig. 2(b), that for the Se-incorporated ATSe crystals, the peak features of $As_2(Te_{0.6}Se_{0.4})_3$ are quite similar to those of As_2Te_3 with α-As_2Te_3 phase. For the higher Se-incorporated sample of $As_2(Te_{0.4}Se_{0.6})_3$, most peak features are similar to those observed in As_2Te_3 and $As_2(Te_{0.6}Se_{0.4})_3$,

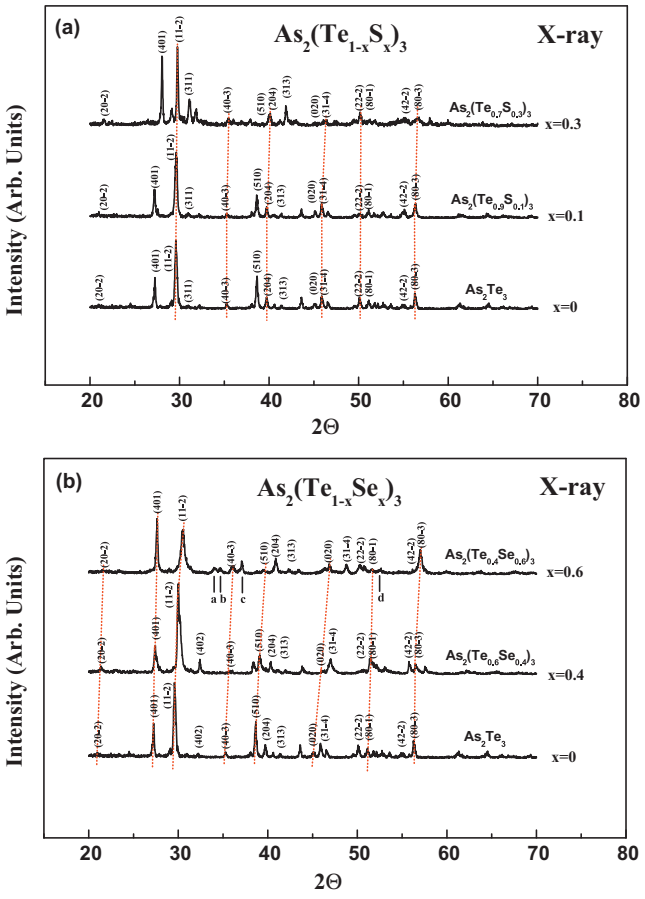

Fig. 2. X-ray diffraction patterns of S- and Se-incorporated $As_2(Te_{1-x}S_x)_3$ and $As_2(Te_{1-x}Se_x)_3$ crystals. (a) Diffraction curves of As_2Te_3, $As_2(Te_{0.9}S_{0.1})_3$, and $As_2(Te_{0.7}S_{0.3})_3$. (b) Diffraction patterns of As_2Te_3, $As_2(Te_{0.6}Se_{0.4})_3$, and $As_2(Te_{0.4}Se_{0.6})_3$.

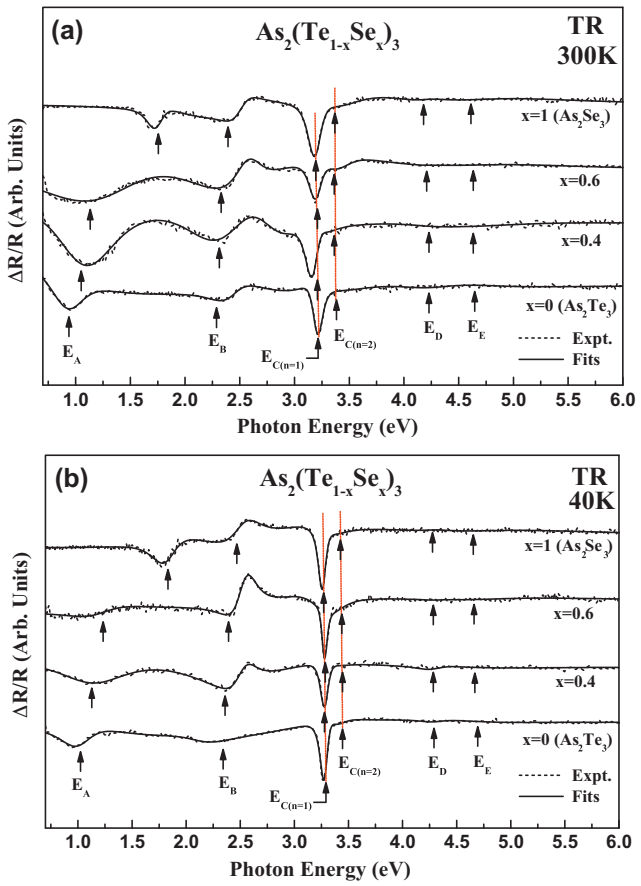

Fig. 3. Experimental TR spectra of $As_2(Te_{1-x}Se_x)_3$ ($0 \le x \le 1$) at (a) 300 K and (b) 40 K. The dashed lines are the experimental data and solid lines are the least-square fits of Eq. (2) to the experimental data. The obtained transition energies are indicated with arrows.

whereas some other different diffraction peaks denoted as a, b, c, and d are observed. These peak features may come from the monoclinic As_2Se_3 with different crystal symmetry (i.e. $C_{2h}{}^5$-$P2_1/n$) [12]. The $As_2(Te_{0.4}Se_{0.6})_3$ compound may crystallize in the mixed phases of major α-As_2Te_3 and a little As_2Se_3 phase. The values of lattice parameters for the crystalline $As_2(Te_{1-x}S_x)_3$ $0 \le x \le 0.3$ and $As_2(Te_{1-x}Se_x)_3$ $0 \le x \le 0.6$ series can be analyzed by fitting the diffraction data to an equation appropriate for the monoclinic system expressed as [17]:

$$\frac{1}{d_{hkl}^2} = \frac{1}{\sin^2\beta}\left(\frac{h^2}{a^2} + \frac{k^2\sin^2\beta}{b^2} + \frac{l^2}{c^2} - \frac{2hl\cos\beta}{ac}\right) \quad (1)$$

where a, b, and c are lattice constants, h, k, and l are Miller indices, and d_{hkl} is the interplanar spacing. The various interplanar distances d_{hkl} can be calculated from the marked diffraction peaks indicated in Fig. 2 by Bragg's law. The lattice parameters can be obtained by fitting Eq. (1) to the calculated d_{hkl} values. It can be accomplished by a Jandel SigmaPlot mathematical software which provides up to 25 parameters and 20 variables in one fitting formula [14]. A good fitting result leads to a standard deviation within ±0.01%. Listed in Table 1 are the fitted results of lattice parameters of the S- and Se-incorporated ATS and ATSe series crystals together with the reported values of As_2Te_3 included for comparison [16]. It is similar to the general crystallographic trend, the higher S- and Se-contained crystals show smaller lattice constants of a, b, and c for the ATS and ATSe chalcogenide systems. The unit-cell volume also reveals reduction for the higher sulfur- and selenium-incorporated As_2Te_3 seen in Table 1.

Table 1
The lattice parameters of S- and Se-incorporated $As_2(Te_{1-x}S_x)_3$ $0 \le x \le 0.3$ and $As_2(Te_{1-x}Se_x)_3$ $0 \le x \le 0.6$ compounds. The values of lattice parameters of previous α-As_2Te_3 (Ref. [16]) are also included for comparison.

Material	a (Å)	b (Å)	c (Å)	β (°)	Volume (Å^3)
As_2Te_3[a]	14.360 ± 0.016	4.008 ± 0.005	9.887 ± 0.013	94.97 ± 0.10	566.91
$As_2(Te_{0.9}S_{0.1})_3$[a]	14.35 ± 0.02	4.007 ± 0.006	9.886 ± 0.014	95.00 ± 0.10	566.28
$As_2(Te_{0.7}S_{0.3})_3$[a]	14.12 ± 0.09	4.005 ± 0.011	9.745 ± 0.023	94.80 ± 0.50	549.15
$As_2(Te_{0.6}Se_{0.4})_3$[a]	14.26 ± 0.03	3.952 ± 0.013	9.725 ± 0.032	94.58 ± 0.22	546.31
$As_2(Te_{0.4}Se_{0.6})_3$[a]	14.18 ± 0.04	3.908 ± 0.021	9.533 ± 0.064	94.54 ± 0.47	526.62
As_2Te_3[b]	14.339 ± 0.001	4.006 ± 0.005	9.873 ± 0.005	95.0	564.96

[a] This work.
[b] Ref. [16].

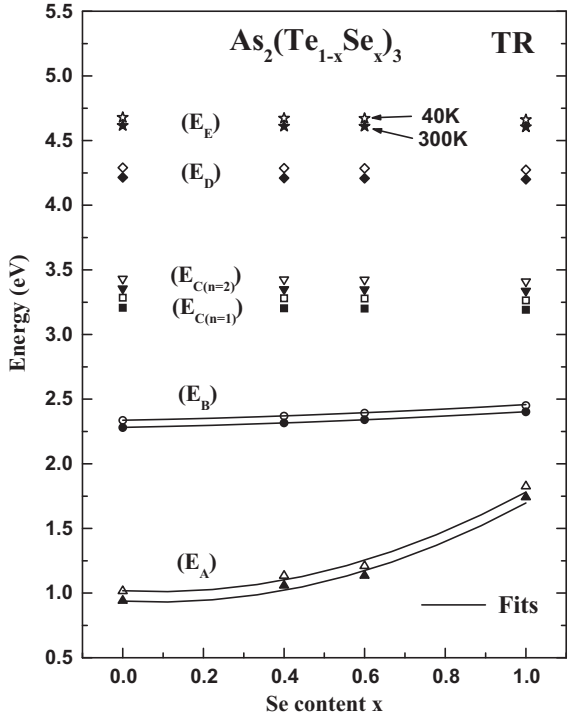

Fig. 4. Composition dependences of transition energies of E_A, E_B, $E_{C(n=1)}$, $E_{C(n=2)}$, E_D, and E_E features in the ATSe compounds.

Fig. 3 shows the thermoreflectance spectra of the ATSe series crystals of As_2Te_3, $As_2(Te_{0.6}Se_{0.4})_3$, $As_2(Te_{0.4}Se_{0.6})_3$, and As_2Se_3 in the energy range of 0.7–6 eV at (a) 300 K and (b) 40 K, respectively. The dashed lines are the experimental curves and solid lines are the least-square fits of the Lorentzian line-shape function appropriate for the interband transitions expressed as [18]:

$$\frac{\Delta R}{R} = \mathrm{Re}\left[\sum_{i=1}^{n} A_i e^{j\phi_i}(E - E_i + j\Gamma_i)^{-2}\right] \quad (2)$$

to the experimental data, where A_i and ϕ_i are the amplitude and phase of the line shape, and E_i and Γ_i are the energy and broadening parameter of the interband transitions. The energy values of the interband transition features can be analyzed by fitting Eq. (2) to the experimental TR spectra. The obtained transition energies are indicated with arrows. There are about four interband transition features (denoted as E_A, E_B, E_D, and E_E) as well as one prominent excitonic series [denoted as $E_{C(n=1)}$ and $E_{C(n=2)}$] which can be detected in each TR spectrum of the ATSe series samples at 40 and 300 K. As the general semiconductor behavior, each transition feature of $E_A - E_E$ in the ATSe compounds shows an energy blue-shift behavior with respect to the decrease of temperatures from 300 to 40 K. The TR feature of $E_{C(n=1)}$ in the excitonic series of the ATSe crystals also reveals a narrowing of the line width when decreasing the temperatures from 300 to 40 K. The fitted values of transition energies in the ATSe series samples using Eq. (2) at 40 and 300 K are depicted as various data points shown in Fig. 4. For E_A and E_B, the compositional dependences of transition energies in the ATSe system obviously show an energy blueshift behavior with respect to the increase of Se composition. The features of E_C, E_D, and E_E do not show clear energy blueshift behavior with the increase of the selenium content in the ATSe system. The features of E_C, E_D, and E_E reveal very weak electronic coupling between the arsenic and chalcogen atoms when the substitution of the Te and Se atoms in the ATSe system. The E_C, E_D, and E_E features are correlated with the interband transitions originated from the largely

Table 2
The compositional dependence of transition energies of E_A and E_B in the Se- and S-incorporated $As_2(Te_{1-x}Se_x)_3$ and $As_2(Te_{1-x}S_x)_3$ compounds at 300 and 40 K. The parameters are obtained by fitting the expression $E(x) = E(0) + bx + cx^2$ to the determined values of interband transition energies.

Material system	Feature	$E(0)$ (eV)	b	c	T (K)
$As_2(Te_{1-x}Se_x)_3$, $(0 \le x \le 1)$	E_A	0.938	−0.163	0.922	300
		1.108	−0.165	0.928	40
	E_B	2.281	0.065	0.057	300
		2.336	0.061	0.061	40
$As_2(Te_{1-x}S_x)_3$, $(0 \le x \le 1)$	E_A	0.938	0.92	0.60	300
		1.108	0.92	0.57	40
	E_B	2.281	0.068	0.121	300
		2.336	0.065	0.117	40

As–As bonds. Compositional dependence of transition energies of E_A and E_B in the $As_2(Te_{1-x}Se_x)_3$ system can be described with the following expression [19]:

$$E(x) = E(0) + bx + cx^2 \quad (3)$$

This relation is customary used to express the composition-dependent gap energy for the direct band gaps in mixed III–V semiconducting compounds, where c is the bowing parameter [19]. The theoretical considerations concerning bowing of the band gap in alloys is still somewhat unclear, but seems to agree that there is a contribution to energy gap bowing as a result of the nonlinear dependence of the crystal potential on the properties of the component ions but the bowing is independent of local potential fluctuations. The fitted results of E_A and E_B in the ATSe system are shown as the solid curves depicted in Fig. 4. The obtained values of $E(0)$, b, and c are given in Table 2. The energy variation for the E_A feature with the alteration of the Se composition shows a faster energy shift than that of the E_B feature. This result confirms that E_A and E_B are of different origins. The E_A transition in the ATSe reveals stronger electronic coupling in the substitution of the Te and Se atoms. It may come from the chalcogen–chalcogen bonds in the diarsenic trichalcogenides. The E_B feature presents weaker electronic coupling and smaller energy shift than those of the E_A transition. The E_B feature can be inferred to originate from the chalcogen lone-pair electrons to As p^* antibonding states. Transition energies of the excitonic series of $E_{C(n=1)}$ and $E_{C(n=2)}$ for the ATSe can be further analyzed by using Rydberg series [20]:

$$E_n = E_\infty - \frac{R_y}{n^2}, \quad n = 1, 2, 3, \ldots, \quad (4)$$

where R_y is the effective Rydberg constant, and E_∞ is the threshold energy of the excitonic sequence. According to the analyses of transition energies of $E_{C(n=1)}$ and $E_{C(n=2)}$ in the ATSe, the values of effective Rydberg constant R_y and threshold energy E_∞ at 40 K (300 K) are determined to be $R_y = 0.196$ eV (0.196 eV) for all the $As_2(Te_{1-x}Se_x)_3$ $(0 \le x \le 1)$ crystals, and $E_\infty = 3.480$ (3.404), 3.474 (3.398), 3.472 (3.396), and 3.459 eV (3.386 eV) for As_2Te_3, $As_2(Te_{0.6}Se_{0.4})_3$, $As_2(Te_{0.4}Se_{0.6})_3$, and As_2Se_3, respectively. The excitonic binding energy of $E_{C(n=2)}$ by Eq. (4) is about $R_y/4 \approx 0.049$ eV, which is higher than that of the thermal energy (kT) at room temperature (~26 meV). It means that the excitonic feature of $E_{C(n=2)}$ in the ATSe do not completely dissociate at 300 K, and can be detected in the room-temperature TR spectra as shown in Fig. 3(a). The E_C features of the diarsenic trichalcogenides [i.e. $E_{C(n=1)}$ and $E_{C(n=2)}$] can be regarded as an interband excitonic series originated from As p bonding state to As p^* antibonding states occurred at Γ point of the Brillouin zone.

Fig. 5 shows the experimental TR spectra of the ATS series compounds of As_2Te_3, $As_2(Te_{0.9}S_{0.1})_3$, $As_2(Te_{0.7}S_{0.3})_3$, and As_2S_3 at (a) 300 K and (b) 40 K, respectively. The dashed lines are the TR data and the solid lines are the least-square fits of Eq. (2), which yield

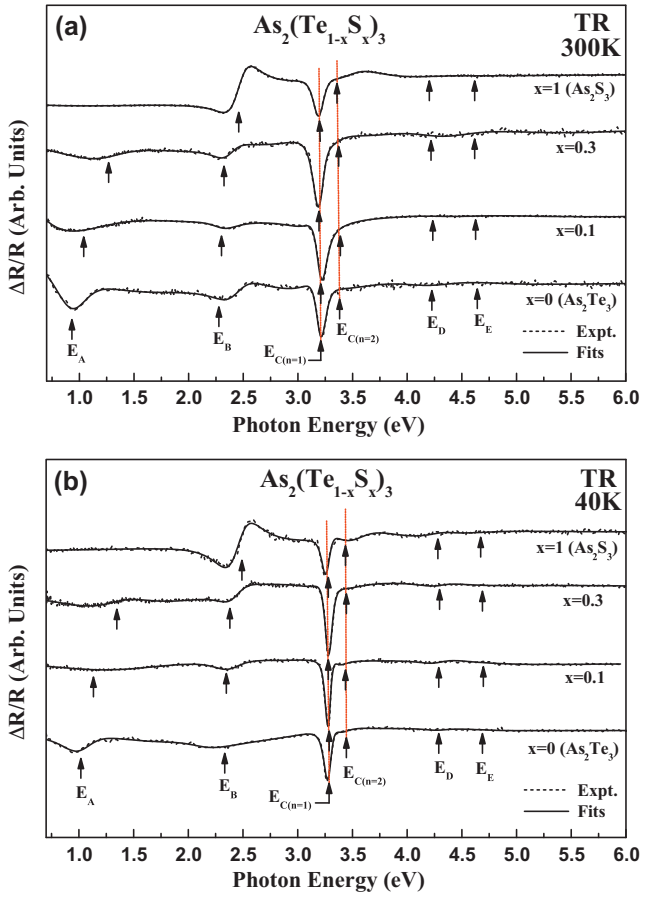

Fig. 5. Experimental TR spectra of $As_2(Te_{1-x}S_x)_3$ ($0 \le x \le 1$) at (a) 300 K and (b) 40 K. The dashed lines are the experimental data and solid lines are the best fits of Eq. (2).

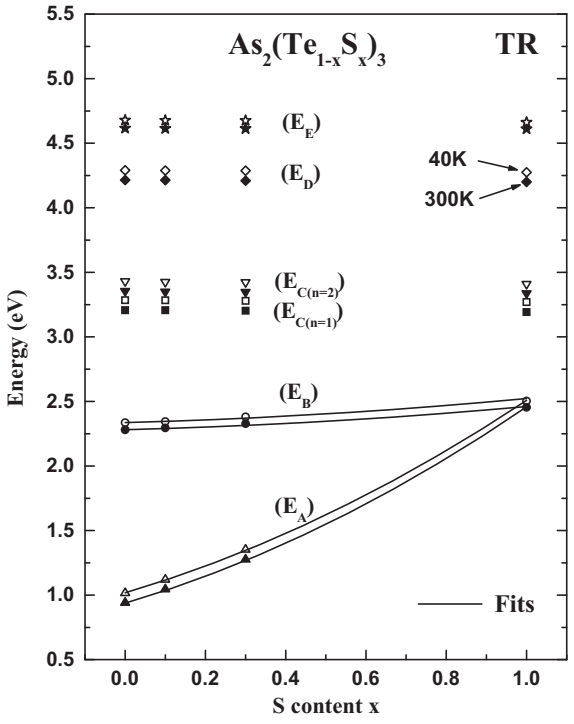

Fig. 6. Composition dependences of transition energies of E_A, E_B, $E_{C(n=1)}$, $E_{C(n=2)}$, E_D, and E_E features in the ATS compounds.

transition energies as indicated by arrows. Observed in the experimental results of the ATS system in Fig. 5, the spectral curves and interband transitions of the ATS are quite similar to those of the ATSe system shown in Fig. 3 except that the E_A feature is detected in all the ATSe and ATS compounds but is not detected in the As_2S_3 sample in the ATS system. As shown in Fig. 5(a) and (b), the energy separations of the E_A and E_B transitions reveal shrinkage with increasing the S compositions in the ATS system. This situation can also be observed in the ATSe system in Fig. 3. For the highest sulfur-incorporated sample of As_2S_3 compound, it is inferred that the valence- and conduction-band states of the E_A and E_B transitions may shift to overlap with each other, which leads to the same transition energy found in the TR measurements. Therefore, the direct band gap of As_2S_3 is approximately determined by the E_B transition not by the E_A feature. From the spectral analyses of Fig. 5(a) and (b), the transition energies of $E_A - E_E$ in ATS also reveal energy blue-shift behavior with the decrease of temperatures from 300 to 40 K. Fig. 6 shows the interband transition energies of E_A, E_B, $E_{C(n=1)}$, $E_{C(n=2)}$, E_D, and E_E of the ATS compounds obtained from the Lorentzian line-shape fits of Eq. (2). The solid lines are the least-square fits of E_A and E_B using Eq. (3). The related fitting parameters are also listed in Table 2. The composition-dependent energy variations of E_A and E_B transitions in the ATS system are higher than those of the ATSe system. It is inferred that the energy values of E_A and E_B with the same x value in the $As_2(Te_{1-x}S_x)_3$ are higher than those of the corresponding values in the $As_2(Te_{1-x}Se_x)_3$ with the same x value [e.g. $E_B(As_2S_3) > E_B(As_2Se_3)$]. The fitting values of the ATSe and ATS in Table 2 also provide useful information to estimate the transition energies of E_A and E_B for the As–S–Se chalcogenides systems. The transition energies of $E_{C(n=1)}$ and $E_{C(n=2)}$ in the ATS system at 40 K (300 K) can be analyzed by using the Rydberg series of Eq. (4). The obtained values of Rydberg constant are R_y = 0.194 (0.194), 0.195 (0.195), and 0.195 eV (0.195 eV) for $As_2(Te_{0.9}S_{0.1})_3$, $As_2(Te_{0.7}S_{0.3})_3$, and As_2S_3, respectively. The obtained threshold energies for the $As_2(Te_{0.9}S_{0.1})_3$, $As_2(Te_{0.7}S_{0.3})_3$, and As_2S_3 at 40 K (300 K) are E_∞ = 3.474 (3.398), 3.472 (3.396), and 3.459 eV (3.386 eV). The value of effective Rydberg constant R_y of E_C in the ATS system is in accordance with that calculated in the ATSe system. This result also confirms that the excitonic binding energies (R_y) of $E_{C(n=1)}$ and $E_{C(n=2)}$ are independent of the inter-substitution of the chalcogen atoms in the ATS and ATSe series compounds. The E_C feature is inferred to originate from the As–As bonding in the diarsenic trichalcogenides. The values of threshold energy (direct gap) of E_C for all the ATS and ATSe systems present slight red shift with the increase of S or Se compositions in the chalcogenides systems. This behavior is different from the composition-dependent energy variations for the E_A and E_B features in ATS and ATSe. The crystallographic structure for monoclinic As_2Te_3 (symmetry: $C_{2h}{}^3$–$C2/m$) and that of monoclinic orpiment As_2S_3 and As_2Se_3 (symmetry: $C_{2h}{}^5$-$P2_1/n$) presents slight structural difference in the atomic arrangements. Each S (Se) atom in the orpiment structure is bonded to two nearest-neighbor As atoms with a bond angle close to 90° and the As atoms are coordinated to three S (Se) atoms in a triangular pyramidal unit [21]. The specific feature for the As_2S_3 and As_2Se_3 structure is the triangular pyramidal units connected with one another to form "helical chains" [6,22]. The helical chains connect together across the weaker-bonded bridging S (Se) atoms to form layers bonded by van der Waals force. Because the elements in the ATS (ATSe) system undergo a structural change from As_2Te_3 to As_2S_3 (As_2Se_3) to construct helical chains, the E_C transition by the As–As bonding may present nearly invariant but slightly unusual red shift of energies with increasing the S (Se) compositions observed in the TR spectra of ATS (ATSe). For As_2Se_3 and As_2S_3 with the same orpiment structure [23], the transition energies of $E_{C(n=1)}$ and $E_{C(n=2)}$ of these two chalcogenides should be

equal. This result can be evident from the similar energy values of E_C features analyzed from the TR spectra of Fig. 3 (As_2Se_3) and Fig. 5 (As_2S_3).

The electronic structures of As_2Te_3, As_2S_3, and As_2Se_3 had ever been studied by X-ray photoemission spectroscopy (XPS), density-of-states (DOS) calculations, and band-structure calculations [21,24]. The band structure of the diarsenic trichalcogenides consists of several band contributions of lowest *s* band, valence band, and conduction band. The *s* band for the orpiment As_2S_3 and As_2Se_3 consists of lower chalcogen (S or Se) *s* orbital and higher As *s* state with energies ranging from −15 eV to −10 eV shown by two separated peaks in the XPS spectra [24]. For As_2Te_3, the *s* band block differs from that of the orpiment As_2S_3 and As_2Se_3, where Te *s* orbital overlaps with arsenic *s* state to form a broadened peak ranging from −15 eV to −10 eV depicted in the XPS spectrum [24]. For the valence and conduction band structures, the band contributions of As_2Te_3 are similar to those of As_2S_3 and As_2Se_3. For valence band, the main blocks of As_2X_3 (X = S, Se, Te) consist of lower chalcogen X bonding like *p* orbitals together with nonbonding X *p* lone-pair electrons positioned at the valence-band top. The calculated results of DOS by charge density also revealed a small amount of As *p* bonding states located at the valence-band edge as well [8]. The main frame of the valence band of As_2X_3 hence consists of X *p* bonding states at the lowest energy band. The chalcogen *p* lone-pair electrons together with a small amount of electron density of the As *p* bonding states positioned at the top of valence band. As_2Te_3, As_2Se_3, and As_2S_3 are direct semiconductors and their optical gaps derived from the TR experiments are 0.938 eV for As_2Te_3, 1.745 eV for As_2Se_3, and 2.454 eV for As_2S_3, respectively. For the conduction-band structure, there are three dominant antibonding blocks consisted in the conduction band of As_2X_3. The band portion of the conduction-band minimum consists of the dominant X p^* states mixed with small proportion of As s^* antibonding states. The higher conduction-band block mainly comes from As p^* antibonding states.

Table 3
Proposed assignments of particular E_A, E_B, E_C, E_D, and E_E features to different interband transitions of series in the Se- and S-incorporated $As_2(Te_{1-x}Se_x)_3$ and $As_2(Te_{1-x}S_x)_3$ compounds.

Features	Transition assignments of interband transitions
E_A	X *p* lone-pair electrons → X p^* antibonding states (Direct band gaps of As_2Te_3 and As_2Se_3)
E_B	X *p* lone-pair electrons → As p^* antibonding states (Direct band gap of As_2S_3)
$E_{C(n=1)}$, $E_{C(n=2)}$	As *p* bonding states → As p^* antibonding states (Excitonic series of ATS and ATSe)
E_D	As *p* bonding states → As p^* antibonding states (higher-lying interband transition of ATS and ATSe)
E_E	As *p* bonding states → As p^* antibonding states (higher lying interband transition of ATS and ATSe)

Based on the experimental analyses of TR measurements together with those of previous band-structure and DOS calculations [21,24], a probable band scheme accounting for the electronic structure of As_2Te_3, As_2Se_3, and As_2S_3 is proposed and depicted in Fig. 7. The highest-energy block for As_2X_3 (X = S, Se, and Te) is As p^* antibonding state. The conduction-band bottom of As_2X_3 consisted of the main contribution of chalcogen X p^* antibonding states mixed with a little As s^* antibonding state. The band contribution for the valence-band top of As_2Te_3, As_2Se_3, and As_2S_3 is coming from the same electronic state, which may be the chalcogen X (Te, Se, and S) *p* lone-pair electron. Following by the X *p* lone-pair electrons, they are the band blocks of As *p* bonding states and chalcogen X *p* bonding states, which construct the main frame of the valence band. For the *s* band, As *s* bonding states are higher in energy with respect to that of the X *s* bonding states for As_2Se_3 and As_2S_3. For As_2Te_3, the As *s* bonding and X *s* bonding states are overlapped to form a broadened peak observed in the XPS measurements [24]. The direct band gaps derived from the energy

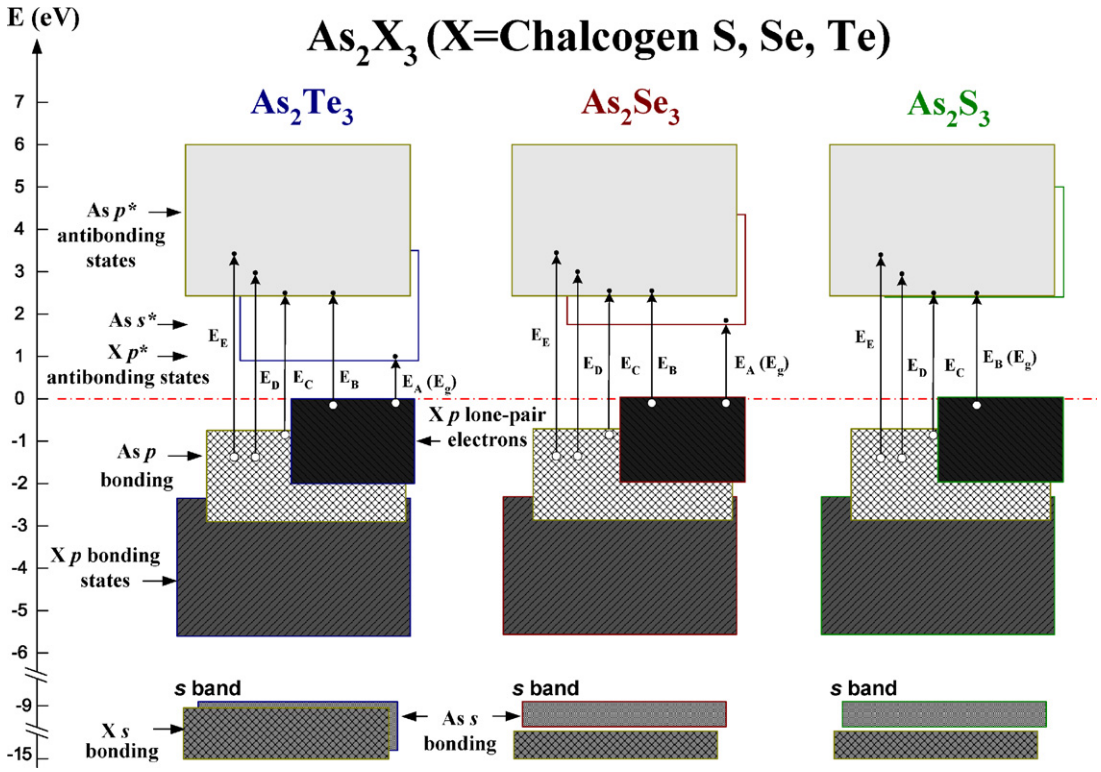

Fig. 7. The probable band-structure schemes of As_2Te_3, As_2Se_3, and As_2S_3. The assignments of the interband transition features of TR are indicated.

difference between the valence-band top and conduction-band bottom are 0.938 eV for As_2Te_3, 1.745 eV for As_2Se_3, and 2.454 eV for As_2S_3, respectively. With increasing the Se and S compositions in the ATSe and ATS series compounds, the band block of X p^* antibonding states (at conduction-band bottom) moves to higher energy to render a larger band gap of E_A shown in Fig. 7. For As_2S_3, the conduction-band bottom of X p^* antibonding state shifts even higher to align with the band edge of the As p^* antibonding states. The band gap of As_2S_3 is hence determined by the E_B transition of S p lone-pair electrons → As p^* antibonding states. The transition assignments of E_A, E_B, E_C, E_D, and E_E features are also depicted in Fig. 7 and which are summarized in Table 3 for comparison. The excitonic series of E_C originates from As p bonding states to As p^* antibonding states at Γ point due to the nearly energy invariant character with the inter-substitution of S, Se, and Te in the diarsenic trichalcogenides. The E_D and E_E features are assigned to the interband transitions of As p bonding states → As p^* antibonding states similar to the E_C feature. This assignment can be referred to the temperature- and composition-dependent energy shift of the E_D and E_E features in the ATSe and ATS systems. The energy-variation behavior of E_D and E_E is similar to that of the E_C excitonic series in the diarsenic trichalcogenides.

4. Summary

Optical properties of $As_2(Te_{1-x}Se_x)_3$ and $As_2(Te_{1-x}S_x)_3$ have been characterized by TR experiments in the energy range from NIR to UV region. Composition-dependent energy variations of the band-edge transitions of ATSe and ATS series are evaluated. The band-edge nature of As_2S_3 shows to be somewhat different from that of As_2Se_3 and As_2Te_3. The band-edge transition of As_2S_3 is originated from chalcogen p lone-pair electrons → As p^* antibonding states, which possesses a larger energy gap than those of the As_2Se_3 and As_2Te_3 (originated from chalcogen p lone-pair electrons to chalcogen p^* antibonding states). From the X-ray and TR experiments it was concluded that As_2Te_3 and As_2Se_3 (or As_2S_3) exhibit slight difference in the crystal structure while they possess comparable bonding structure in valence band and conduction band. The band schemes for the As_2Te_3, As_2Se_3, and As_2S_3 chalcogenides are proposed. The possible origins for the interband transitions of the diarsenic trichalcogenides are assigned. The band variation in between the $As_2(Te_{1-x}Se_x)_3$, $As_2(Te_{1-x}S_x)_3$ and $As_2(se_{1-x}S_x)_3$ series compounds is hence being realized.

Acknowledgment

The author would like to acknowledge the research funding supported from the National Science Council of Taiwan under the contract no. NSC98-2221-E-011-151-MY3.

References

[1] N.S. Platakis, H.C. Gatos, Phys. Status Solidi A 13 (1972) K1.
[2] J.A. Savage, J. Non-Cryst. Solids 11 (1972) 121.
[3] K. Weiser, M.H. Brodsky, Phys. Rev. B 1 (1970) 791.
[4] J. Cornet, D. Rossier, J. Non-Cryst. Solids 12 (1973) 85.
[5] T.J. Scheidemantel, J.V. Badding, Solid State Commun. 127 (2003) 667.
[6] C.J. Brabec, Phys. Rev. B 44 (1991) 13332.
[7] O. Madelung, Semiconductors—Basic Data, 2nd ed., Springer, New York, 1996, p. 205.
[8] E. Tarnow, A. Antonelli, J.D. Joannopoulos, Phys. Rev. B 34 (1986) 4059.
[9] H. Hisakunia, K. Tanaka, Appl. Phys. Lett. 65 (1994) 2925.
[10] A.V. Kolobov, V. Lyubin, T. Yasuda, K. Tanaka, Phys. Rev. B 55 (1997) 23.
[11] I. Abdulhallm, R. Beserman, R. Weil, Phys. Rev. B 40 (1989) 12476.
[12] C.C. Wu, J. Appl. Phys. 101 (2007) 063533.
[13] R.A. Laudise, The Growth of Single Crystals, Prentice-Hall Inc., Englewood Cliffs, NJ, 1970 (Chapter 5).
[14] SigmaPlot Scientific Graph System, Jandel Corporation Version 1.01.
[15] C.H. Ho, H.W. Lee, Z.H. Cheng, Rev. Sci. Instrum. 75 (2004) 1098.
[16] G.J. Carron, Acta Cryst. 16 (1963) 338.
[17] B.D. Cullity, S.R. Stock, Elements of X-Ray Diffraction, 3rd ed., Prentice-Hall Inc., New Jersey, 2001.
[18] F.H. Pollak, H. Shen, Mater. Sci. Eng. R: Rep. 10 (1993) 275.
[19] J.A. Van Vechten, T.K. Bergstresser, Phys. Rev. B 1 (1970) 3351.
[20] C.H. Ho, P.C. Yen, Y.S. Huang, K.K. Tiong, Phys. Rev. B 66 (2002) 245207.
[21] D.W. Bullet, Phys. Rev. B 14 (1976) 1683.
[22] A.C. Stergiou, P.J. Rentzeperis, Z. Kristallogr. 173 (1985) 185.
[23] I. Chen, Phys. Rev. B 8 (1973) 1440.
[24] S.G. Bishop, N.J. Shevchik, Phys. Rev. B 12 (1975) 1567.